Phases and phase transformations in nanocrystalline ZrO_2

D. Vollath[1,*], F. D. Fischer[2], M. Hagelstein[3] and D. V. Szabó[4]

[1]*NanoConsulting, Primelweg 3, D-76297, Stutensee, Germany;* [2]*Montanuniversität Leoben, Institute of Mechanics, Erich Schmid Institute of Materials Science, Austrian Academy of Sciences, Franz-Josef-Strasse 18, A-8700, Leoben, Austria;* [3]*Forschungszentrum Karlsruhe, Institut für Synchrotronstrahlung, P.O. Box 3640, D-76021, Karlsruhe, Germany;* [4]*Forschungszentrum Karslruhe, Institut für Materialforschung III, P.O. Box 3640, D-76021, Karslruhe, Germany;* *Author for correspondence (E-mail: dieter.vollath@ nanoconsulting.de)*

Abstract

Starting from results from He-pycnometry, electron diffraction, Extended X-ray Absorption Fine Structure Spectroscopy and Perturbed Angular Correlation Spectroscopy the phase transformations and structures of zirconia are described. From a comparison of these results with those obtained on other oxide nanoparticles it is concluded that the phases and structure of nanoparticles are different compared to those of coarse-grained material. The difference of the transformation temperature of bare and coated nanoparticles was used to estimate enthalpy and entropy of the tetragonal $\rightarrow$ monoclinic transformation for nanoparticulate zirconia. By comparison with results obtained from other nanocrystalline oxides, the following rules were derived: Provided the particles are sufficiently small, particles made of materials showing phase transitions crystallize in the high temperature structure. However, compared to coarse-grained materials of the same structure, the density of nanoparticles is reduced. A first estimation limits this phenomenon to particle sizes well below 10 nm. Those nanoparticles follow the generalized phase diagram postulated by Tammann.

Introduction

Undoped coarse-grained zirconia, ZrO_2, shows a series of phase transformations. At high temperatures it crystallizes in the cubic fluorite structure, at lower temperatures it transforms into the tetragonal one. At room temperature the stable structure is monoclinic. The cubic phase exhibits the highest, the monoclinic one the lowest density (Massalski, 1990). The temperature of the different phase transformations decreases with decreasing grain size. Furthermore, compressive stresses promote the stability of the phases with higher density. This study is a rigorous thermodynamic evaluation of earlier published experimental data (Vollath & Sickafus, 1992; Forker et al., 2000; Hagelstein et al., 2001; Vollath et al., 2001) on the structure of zirconia nanoparticles. It will be tried to pose these results into a broader context by summarizing data stemming from different experimental techniques and comparison with similar results from other oxides.

For this study, undoped nanocrystalline zirconia, n-ZrO_2, with particle sizes around 5 nm, were

synthesized as bare particles and with alumina, Al_2O_3, coating, using the microwave plasma process (Vollath & Sickafus, 1992; Vollath & Szabó, 1994). It is one of the main characteristics of this process that the particles leave the reaction zone with electric charges of equal sign. This avoids agglomeration leading to extremely narrow particle size distributions and makes the coating of the individual particles possible. Coating with alumina keeps the zirconia particles apart and, therefore, avoids sintering and grain growth of the zirconia phase at elevated temperatures. Additionally, due to the differences in the thermal expansion the alumina coating causes a hydrostatic stress state on the core, especially during the phase transformation. The morphology and structure of the particles were studied by electron microscopy, X-ray, and electron diffraction. The density of the bare particles was determined using He-pycnometry. HfO_2, TiO_2, and Fe_2O_3 used for comparison of the results were produced by the same microwave plasma process.

In addition to these standard procedures, Extended X-ray Absorption Fine Structure Spectroscopy (EXAFS) measurements probing the interatomic distances and the number of next nearest neighbors (Koningsberger & Prins, 1987) in the lattice of the specimen were applied, giving very detailed information on the local structure. The experimental results were evaluated by comparison with calculated results obtained from different structure models of zirconia (Hagelstein et al., 2001).

The local symmetry around the Zr^{4+} ions was investigated by perturbed angular correlation (PAC) measurements (Frauenfelder & Steffen, 1974; Catchen, 1995) of the electric quadrupole interaction in the temperature range from 290 K to 1400 K. A β-emitter, ^{81}Hf, with a half-life time of 45 d, produced by thermal neutron irradiation of ^{180}Hf, was used as nuclear probe. Zirconium chloride, used in this study as a precursor for synthesis, contained ca. 2% Hf (Forker et al., 2000; Vollath et al., 2001). As Zr and Hf are chemically very similar and their ionic radii are nearly equal, this does not lead to a significant distortion of the lattice. The PAC spectra of the nanocrystalline compound were evaluated by comparison with those of the coarse-grained material. PAC spectra carry mainly information on the local symmetry at the probe site. On the

other hand, high-resolution electron microscopy and electron diffraction are used to analyze the lattice as a whole. These results together provide detailed information both on local and global structure and symmetries. Additionally, the influence of coating on the transformation is evaluated experimentally and theoretically leading to a first estimation of the free enthalpy of the monoclinic $\rightarrow$ tetragonal transformation. The findings are similar to those of Wang et al. (2004), who found at room temperature cubic zirconia in thin films with a few nanometer thickness. Similarly, cubic zirconia was found by Kao & Gorman (1990) in pure zirconia particles with sizes below 40 nm and by Moulzolf et al. (1997) in thin film layers with a thickness of less than 40 nm. The comparison of these results with similar ones from other oxides published in literature, leads to new insights about phases in nanoparticles. Additionally, to demonstrate that the presented results are not restricted to zirconia, similar data obtained on TiO_2, HfO_2, and Fe_2O_3 are used to underpin that a generalization of the interpretations may be allowed.

Experimental results

The results of He-pycnometry density measurements on loosely pressed powders of the bare material together with the X-ray density of the cubic structure are summarized in Table 1.

The value for the X-ray density was, in this and all the other cases, calculated on the basis of the structural information given in the Inorganic Crystal Structure Database (ICSD) and JCPDS data. A relative density of 0.65 seems to be erroneous. Therefore, these measurements were repeated a few times with different specimens. The results were reproducible. Furthermore, similarly low values were found for other nanoparticulate oxides. Hypothetically, the density may be reduced by a surface layer of zirconium hydroxide with a density of roughly 3.5 g cm ^{3}. A hydroxide surface layer of 0.5 nm would reduce the density

Table 1. Density of cubic, nanocrystalline zirconia in comparison to the X ray density

	Nanoparticles (g cm^{-3})	X ray density (g cm^{-3})	Relative density of nanoparticles
c ZrO_2	3.8	5.86	0.65

to 5.2 g cm ^{3} and a surface layer of 1 nm to 4.7 g cm ^{3}. However a surface layer of that thickness should be visible in the electron micrographs. It was never observed. Figure 1 displays an electron micrograph of zirconia particles. Some of these particles are oriented in a way that lattice fringes are visible.

None of these particles show a surface layer. Therefore, the hydroxide hypotheses is excluded definitely. The crystal structure of the material was determined by electron and X-ray diffraction. Because of the limited accuracy of these methods in the case of nanoparticles, it was not possible to decide if the material was crystallized in the cubic or tetragonal structure. As an example for the structure determination, Figure 2 displays an X-ray diffraction spectrum of uncoated zirconia nanoparticles. Because of the small grain size, the diffraction lines are extremely broad. Additionally, the diffraction pattern does not show any indication for the existence of a second phase.

Figure 3 displays an electron micrograph of an alumina coated particle. From the lattice fringes visible in these micrographs and the electron diffraction patterns it is obvious that the particle cores are well crystallized. For bare and coated zirconia electron diffraction indicated, within the limited precision of the method, the cubic structure for the material. In all cases the size of the zirconia
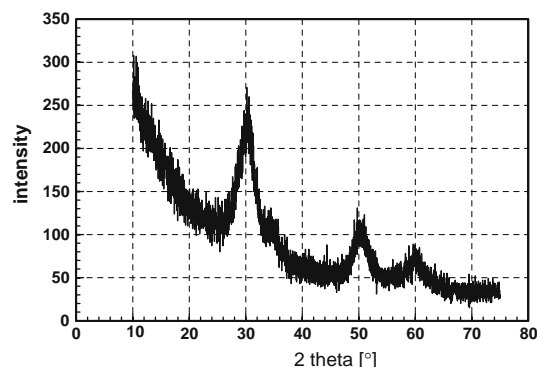

Figure 2. X ray diffraction spectrum of nanocrystalline zirconia. Because of the small particle size, extreme broad line profiles characterise this spectrum.

particles was around 5 nm. The alumina coating, with a thickness of approximately 1 nm, was amorphous. An exact determination of the coating thickness is nearly impossible, because of the poor contrast of this amorphous, low Z material directly adjacent of crystallized zirconia. Therefore, in the following considerations, a thickness of 1 nm is assumed. However, the influence of a thickness variation of ±0.25 nm is studied.

More detailed structural information was obtained using EXAFS (Hagelstein et al., 2001). A comparison of the Fourier transformed EXAFS
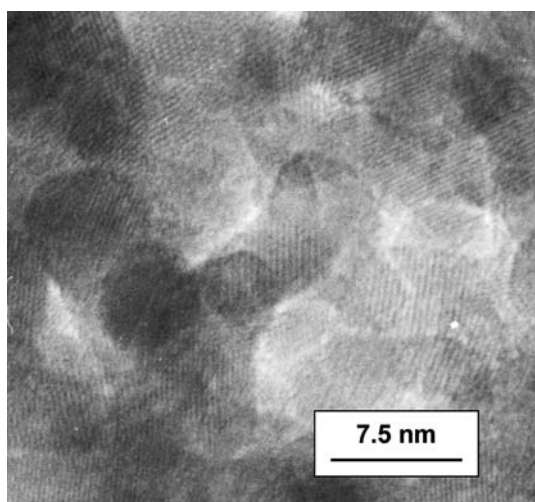

Figure 1. High resolution electron micrograph of uncoated zirconia particles. The lattice fringes show that the particles are not covered with a hydroxide layer of significant thickness.
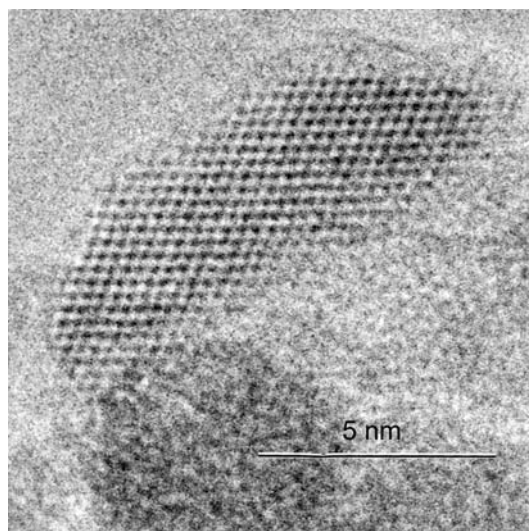

Figure 3. Electron micrograph of an alumina coated zirconia particle.

measurements with calculated model structures of cubic, tetragonal and monoclinic symmetry indicates the cubic structure of the as fabricated material. In the tetragonal structure, two distinctly different radii as compared to a single one for cubic ZrO_2 characterize the nearest Zr–O shell. The experimental data for nanocrystalline ZrO_2 coated with Al_2O_3 does not show any indication for splitting. Additionally, a characteristic double peaked shape of the imaginary part, characteristic for the cubic structure, of the Fourier transformed data is observed experimentally. However, a multiple scattering feature, expected due to the higher symmetry in the cubic structure only, is not found in the experimental data. Its absence is an indication for a disturbance of the symmetry of the ZrO_8 polyhedron. These results together clearly point to the cubic structure of the 'as fabricated' material. Table 2 summarizes experimental and calculated data for the shell radii and coordination numbers (Hagelstein et al., 2001).

A comparison of the measured values with the calculated ones shows drastically reduced coordination numbers. The experimentally found values for the nanocrystalline material are approximately half of the calculated values. In the case of coarse cubic zirconia, replacing of more than 30 at % of zirconium ions by trivalent yttrium reduces the coordination numbers to 5.4. Comparing this theoretically expected value with the experimental one, one could assume a systematically reduced coordination number for about 25%. In nanoparticulate materials, a significant fraction of the ions is at the surface, therefore, a leading to a reduced coordination number. Even taking into account experimental errors and the reduced number of neighbors for Zr ions at the surface, the reduced coordination number found for nanoparticulate zirconia is too small. Obviously, the material has an unusual high concentration of vacancies. The cubic structure, characterized by such a high concentration of vacancies, will be called "defective structure".

On the other hand, this reduced coordination number explains the missing multiple scattering feature in the Fourier transformed spectra and fits well to the reduced value found for the He-density. Furthermore, EXAFS (Hagelstein et al., 2001) results reveal an increase of the radial distance to the O shell with increasing temperature. Table 3 shows these results in detail.

The increase of the radii with increasing temperature as displayed in Table 3 is significant. Independently of experimental uncertainties, the

Table 2. Structure parameters of alumina coated nanocrystalline zirconia at room temperature revealed from EXAFS data measured on Al_2O_3 coated ZrO_2 nanoparticles in comparison to calculated values for the ideal lattice

	Shell	Radial distance $\pm\sigma$ (nm)	Coordination number
Experimental nano ZrO_2/Al_2O_3	Zr O	0.214 ± 0.00076	4.1
	Zr Zr	0.365 ± 0.00089	6.4
Experimental coarse cubic $ZrO_2(Y_2O_3)$	Zr O	0.219 ± 0.00087	5.4
	Zr Zr	0.360 ± 0.0010	10.5
Calculated cubic ZrO_2 after Antonioli et al., 1994	Zr O	0.2238	8
	Zr Zr	0.365	12
Calculated tetragonal ZrO_2 after ICSD entry No. 4275	Zr O	0.207/0.245	4 / 4
Calculated average monoclinic ZrO_2 after ICSD entry No. 6184	Zr O	0.226	8
	Zr Zr	0.367	12

Table 3. Radial distance of the Zr O shell as function of temperature determined with Al_2O_3 coated ZrO_2 specimens

Temperature (K)	Radial distance Zr O (nm)	Radial distance Zr O (nm) as expected due to thermal expansion	Coordination number
300	0.214 ± 0.00076	0.214	4.1
433	0.217 ± 0.00093	0.2142	4.5
533	0.218 ± 0.00095	0.2144	4.6
573	0.218 ± 0.00098	0.2145	4.6

trend of lattice expansion larger than thermal expansion is evident. This indicates partial transition from the cubic to the tetragonal phase. The slight increase of the coordination number is interpreted as a consequence of the transition from a disordered structure to a more ordered one.

Perturbed angular correlation spectra (PAC) reflect the symmetry and strength of the perturbing quadrupole interaction at the place of the nucleus (Schatz & Weidinger, 1996). Therefore, these spectra are characteristic of the crystal structure of the matrix. The PAC spectra of bare and coated zirconia nanoparticles were measured at a series of temperatures (Forker et al., 2000). During irradiation and heating experiments, the material was gastight encapsulated in silica vials. In the temperature range under consideration, the oxygen partial pressure of silica is always higher than the one of zirconia. This ensured that oxygen losses of the zirconia specimen during the experiments are not probable. In line with these considerations is the observation that the white color of the as-produced material did not change to grey or black during these experiments. Comparing the PAC results of nanocrystalline zirconia with the ones of coarse-grained material allows an interpretation. After neutron activation at room temperature, both for the bare and the coated material, the spectra reflect the features of a broad distribution of the quadrupole interaction typically observed in disordered material. As electron diffraction and EXAFS have shown that the as produced material is crystallized in the cubic structure, this phase is denoted as 'disordered cubic'.

With increasing temperature, the transition to the tetragonal and at slightly higher temperature to the monoclinic phase can be seen. A further increase of the temperature to ca. 1400 K leads to the monoclinic $\rightarrow$ tetragonal transformation. The coating does not influence the temperature of this transformation. However, there is a high probability that the temperature of this transformation is already influenced by grain growth or other secondary reactions.

The tetragonal $\rightarrow$ cubic transformation was not accessible, because of a reaction between the specimen and specimen holder. A solid-state reaction of the sample with the SiO_2 sample holder, forming $ZrSiO_4$, occurred. Table 4 summarizes the transformation temperature found for bare and coated particles.

Table 4. Transformation temperature observed for bare and alumina coated zirconia particles determined by PAC measurements

Specimen type	Transformation		
	cubic $\rightarrow$ tetragonal	tetragonal $\rightarrow$ monoclinic	monoclinic $\rightarrow$ tetragonal
Bare particles	400 K	700 K	1400 K
Coated particles	400 K	1300 K	1400 K

The spectra observed after neutron activation at room temperature, showing a broad distribution of the quadrupole interaction, reflect a high degree of disorder, or a lack of symmetry. The dominant contribution to the quadrupole interaction comes from the nearest neighbours of the probe nucleus, ^{181}Ta on Zr^{4+} sites, the O^2 anions. Electron diffraction and EXAFS results for this material clearly showed a phase close to the cubic fluorite structure. Therefore, in the 'as neutron activated' state of these compounds the cations are found at the lattice positions of the fluorite structure; however, in line with the density and EXAFS results, with reduced population of the cation lattice sites. The distribution of quadrupole interactions observed in the PAC spectra, therefore, implies that the anion lattice positions are randomly occupied by a reduced number of oxygen ions. Due to the small scattering power of the oxygen ions, this does not contribute to the electron diffraction pattern. In both the coated and the bare particles, heating of the specimen above 500 K initiates the transformation to the tetragonal structure. Experiments at different temperatures were performed stepwise. Due to the time necessary for measurement, the holding time at each temperature step was in the range between 15 and 20 h.

Additional PAC experiments in which the sample was cycled between an elevated temperature and room temperature demonstrated that during quenching, the tetragonal phase undergoes a back-transformation to a disordered structure. This was taken as indication for the reversibility of the cubic $\rightarrow$ tetragonal transformation. Certainly, at room temperature transformations are very slow. Therefore, one cannot expect completion of the reverse transformations during the measuring time. Additionally, at temperatures above 800 K, an
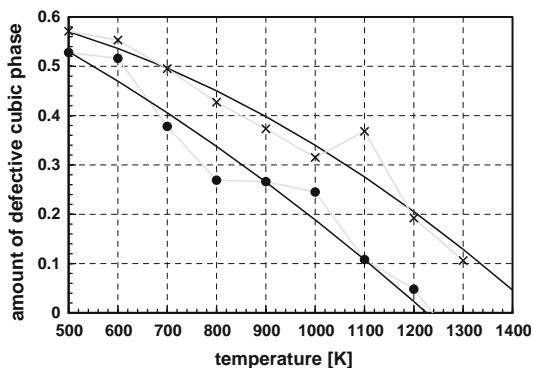
Figure 4. Amount of the defective cubic phase determined by PAC cycling experiments at elevated temperature and after cooling at room temperature. These results indicate at least a partial back transformation tetragonal → cubic during cooling.

influence of some grain growth can not be excluded. Therefore, these experiments only give indications of possible phase transformations. The results demonstrated in Figure 4 show that the transformation 'defective cubic'-tetragonal transformation is – at least – partially reversible. This leads to the conclusion that the observed cubic phase is not a quenched high temperature phase. However, as the defective cubic structure shows a random population of a reduced number of ions on the lattice positions, the identity of this structure after fabrication and after back-transformation is not granted.

Looking at the tetragonal → monoclinic transformation, the two types of specimen behave differently. PAC results show that at about 700 K bare n-ZrO_2 starts to transform from the tetragonal to the monoclinic phase, whereas the coated specimen remains tetragonal up to 1300 K. At 1400 K both types of specimen transform – according to the phase equilibrium – back to the tetragonal structure. The fraction of the tetragonal phase decreases, forming the disturbed cubic one, when the material is cooled from elevated to room temperature. The monoclinic phase does not undergo any phase transformation during cooling.

As the volume change of the cubic → tetragonal transformation is very small, no mechanical confinement was observed, and the transformation temperature of bare and coated particles is the same.

Discussion of the results

As a result of the PAC measurements it was shown that nanoparticulate zirconia exhibits the following phase transformation with increasing temperature:

Cubic → tetragonal → monoclinic
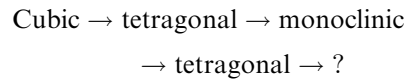
→ tetragonal → ?

Because of an interaction between the specimen and the holder, phase transformations beyond the tetragonal phase were not experimentally accessible.

It was demonstrated that the cubic → tetragonal transformation is at least partly reversible. This was not observed for the other transformations. This lack of reversibility is – with high probability – caused by grain growth in the case of bare particles and a combination of grain growth and solution of alumina in zirconia (Srdic et al., 1999) in the case of coated particles. In any case, the reversibility of the cubic → tetragonal transformation indicates that at room temperature the cubic phase is an equilibrium phase. Furthermore, PAC measurements in combination with electron and X-ray diffraction demonstrated that the cubic phase exhibits after synthesis and after cycling to elevated temperatures a long range ordering with reduced symmetry, caused by a high concentration of vacancies. As the transformation cubic → tetragonal is at least partly reversible, it is assumed that the 'defective'' structure is an equilibrium structure. Finding cubic zirconia at room temperature is not unique. In earlier papers Moulzof et al. (1997) and Wang et al. (2004) found at room temperature cubic zirconia in thin films with a few nanometer thickness. However, like in the results presented in this paper (Wang et al., 2004) showed by a very detailed analysis of the electron diffraction pattern that this cubic phase has a heavily distorted oxygen partial lattice. In pure zirconia particles with sizes below 40 nm, (Kao & Gorman, 1990) were also found in the cubic phase.

The onset of the tetragonal → monoclinic transformation is found at 700 K for bare particles and at 1300 K for alumina coated ones. As the tetragonal → monoclinic transformation is connected with a volume change of ca. 4 vol%, the increase of the transformation temperature for

coated particles may be explained by mechanical confinement leading to the generation of elastic strain energy ΔG_{strain}. Surface coating thwarts the transformation up to a temperature of 1300 K. The transformation condition can be formulated as

$$G_{\text{volume, tetragonal}} + G_{\text{surface, tetragonal}}$$
$$= G_{\text{volume, monoclinic}} + G_{\text{surface, monoclinic}}$$
$$+ \Delta G_{\text{strain}} + F_{\text{transformation}} \qquad (1a)$$

The free enthalpy for the transformation is derived from equation (1a) as

$$G_{\text{volume, tetragonal}} - G_{\text{volume, monoclinic}}$$
$$= -(G_{\text{surface, tetragonal}} - G_{\text{surface, monoclinic}})$$
$$+ \Delta G_{\text{strain}} + F_{\text{transformation}} \qquad (1b)$$

The quantity $\Delta G_{\text{transformation}} = G_{\text{volume, tetragonal}} - G_{\text{volume, monoclinic}}$ is the change of chemical energy due to the transformation. Since also the surface of the specimen is changed, an additional barrier term $\Delta G_{\text{surface}} = G_{\text{surface, tetragonal}} - G_{\text{surface, monoclinic}}$ is active. The difference of the surface energy is described as

$$\Delta G_{\text{surface}} = \Delta\gamma A_{\text{interface}}$$
$$+ \gamma_{\text{coating}}(A_{\text{monoclinic}} - A_{\text{tetragonal}}). \qquad (2)$$

The first term in (2) corresponds to the change of the surface energy on the interface between the core and the coating and is expressed by the surface energy difference term $\Delta\gamma$ and the corresponding surface $A_{\text{interface}}$, for which the reference surface is taken in a small strain setting. The second term meets the change of the outer surface and, therefore, the change of the surface energy on the coating.

The quantity $F_{\text{transformation}}$ denotes a further barrier term occurring due to the rearrangement of the lattice. Since usually $\Delta G_{\text{transformation}}$ is taken from a stress-free specimen, de facto one measures $\Delta G_{\text{transformation}} - F_{\text{transformation}}$. Therefore, it is assumed that this term is included in $\Delta G_{\text{transformation}}$, and the same notation is kept.

The transformation condition as (1a) was introduced by Garvie (1978) and put on a general basis in Fischer & Reisner (1998) and for spherical inclusions in Fischer & Oberaigner (2000), including also the surface energy term (related to the so-called Gibbs-Thomson effect). The strain energy for an inclusion in an infinite matrix with different material properties can be found in (Böhm et al., 1997; Fischer & Böhm, 2005). However, in the case at hand only a coating (a shell) acts as a confinement. The corresponding strain energy can be calculated as

$$\Delta G_{\text{strain}} = V_{\text{particle}} E_{\text{core}} \varepsilon^2 \tilde{f}. \qquad (3)$$

In this formula V_{particle} is the volume of the zirconia core, $\varepsilon = \delta/3$ with $\delta = (V_{\text{monoclinic}} - V_{\text{tetragonal}})/V_{\text{tetragonal}}$. This is the relative volume change during the tetragonal $\rightarrow$ monoclinic transformation. The coefficient $\tilde{f}$ follows as

$$\tilde{f} = \frac{3}{2(1-2v_{\text{core}})} \frac{1}{1 + \frac{E_{\text{core}}}{E_{\text{coating}}} \frac{2(1-2v_{\text{coating}})+(1-v_{\text{coating}})(1-\kappa)^3}{2(1-2v_{\text{core}})[(1-\kappa)^3-1]}}. \qquad (4)$$

E_{core}, E_{coating} are the Young's moduli of the zirconia core and the alumina coating, respectively. The Poisson ratios $v_{\text{core}}, v_{\text{coating}}$ are those of core and coating, respectively. The abbreviation κ is used for $\kappa = (r_{\text{coating}} - r_{\text{core}})/r_{\text{core}}$. The radii r_{coating}, r_{core} are those of the bare and coated particle, respectively. One should keep in mind that the mechanical terms ΔG_{strain} and $\Delta G_{\text{surface}}$ are expressed in MPa and must be transferred to J mol^{-1} via the molar volume. One can also meet the role of the residual stress state due to coating by adding to ε an initial eigenstrain $\Delta\alpha_c \Delta T_c$ with ΔT_c being the difference between the coating temperature and transformation start temperature and $\Delta\alpha_c$ being the difference between the thermal expansion coefficient of the core and coating. A short estimation, however, verifies that $\Delta\alpha_c \Delta T_c$ can be neglected in relation to ε.

With respect to $\Delta G_{\text{transformation}}$ one has to insert the transformation temperatures in the bare and coated case. This leads to a system of two linear equations

$$\Delta G_{\text{transformation}} = \Delta G_{\text{t}\rightarrow\text{m}} = \Delta H_{\text{t}\rightarrow\text{m}}$$
$$- T_{\text{bare}} \Delta S_{\text{t}\rightarrow\text{m}} - \Delta G_{\text{surface}} = 0,$$
$$\Delta G_{\text{transformation}} = \Delta G_{\text{t}\rightarrow\text{m}} = \Delta H_{\text{t}\rightarrow\text{m}} - T_{\text{coated}} \Delta S_{\text{t}\rightarrow\text{m}}$$
$$- \Delta G_{\text{surface}} = \Delta G_{\text{strain}}. \qquad (5)$$

The quantities $\Delta H_{\text{t}\rightarrow\text{m}}$ and $\Delta S_{\text{t}\rightarrow\text{m}}$ are the enthalpy and entropy of the tetragonal – monoclinic transformation, respectively. T_{bare} and T_{coated} are the

transformation temperatures of the bare and the coated particles, respectively.

Looking at the other parameters necessary to evaluate formulae (1) to (5) one realizes the necessity of a large number of material constants to be available. They are E_{core}, $E_{coating}$, ν_{core}, $\nu_{coating}$, $\Delta\gamma$ and γ, $\Delta H_{t\to m}$, $\Delta S_{t\to m}$. Most of them are dependent on the temperature and poorly known or unknown. For monoclinic zirconia, Garvie (1978) gives a value of 1.46 J m^{-2} for γ and uses for the tetragonal phase the value of 1.1 J m^{-2} reported by Livey and Murray (1956). These data are used also by Suresh et al. (2003) and Mayo et al. (2003). These authors assume that the difference $\Delta\gamma = \gamma_{monoclinic} - \gamma_{tetragonal} = 0.35$ J m^{-2} is only slightly temperature dependent. However, in a series of recent papers, McHale et al. (1997) and Navrotsky (2003) give significantly higher values for the surface energy in the different zirconia phases. For the monoclinic phase these authors determined a value of 6.5 J m^{-2}, for the tetragonal phase 2.1 J m^{-2}, and for amorphous zirconia 0.5 J m^{-2}. The situation is similar for alumina. Navrotsky (2003) and McHale et al. (1997) give the values 2.6 J m^{-2} for the α-phase and 1.7 J m^{-2} for the γ-phase. In (Kingery et al., 1976) a value of 0.7 J m^{-2} and for the crystalline material 0.905 J m^{-2} is given for the liquid phase. For amorphous alumina there are no data published. However, looking at the zirconia data from Navrotsky (2003) and McHale et al. (1997), one may assume significantly lower values as compared to the crystalline phases. Additionally, for amorphous alumina such data are absolutely unknown. Taking this situation for the data for surface energies into account, in lack of a sufficiently reliable data basis, the surface energy γ is set to the most common value of 1 J m^{-2}, see (Garvie, 1978) and (Ondracek, 1994). Therefore, the interface energy term $\Delta\gamma = \gamma_{Al_2O_3} - \gamma_{ZrO_2}$ and consequently the first term in (2) was neglected, otherwise, a not existing precision is feigned.

The major questions in this context are: Is $\Delta G_{transformation}$ the same for nanoparticles as for coarse-grained material? Which value should be used as Young's modulus $E_{coating}$ for the alumina coating? Considering these two questions, one realizes the uncomfortable situation of having two equations and three unknown parameters. Therefore, if at all, this evaluation gives answers only for $\Delta S_{t\to m}$ and $\Delta H_{t\to m}$. However, one may not expect any answer for $E_{coating}$ of amorphous alumina. As for $\Delta G_{transformation}$, at least for coarse-grained material, the data are known, $E_{coating}$ was used as free parameter.

For coarse material Zhang et al. (2003) give the most recent values for the free enthalpy of the different phases of zirconia as

$$G_{tetragonal} = -93954.8 + 31.755 * T \quad [\text{Jmol}^{-1}]$$
$$G_{monoclinic} = -99978.8 + 35.898 * T \quad [\text{Jmol}^{-1}]$$
$$(6)$$

Therefore, one obtains for the tetragonal $\to$ monoclinic transformation:

$$\begin{aligned}
\Delta G_{transformation} &= \Delta G_{t\to m} \\
&= G_{tetragonal} - G_{monoclinic} \\
&= 6024 - 4.143 * T \quad [\text{Jmol}^{-1}].
\end{aligned}$$

Using these values for the free enthalpy of transformation one can calculate the transformation temperature using $E_{coating}$ as free parameter. To do this, the value for the volume change during transformation was selected according to (Wang et al., 1995). Additionally, the smallest possible value was estimated from the JCPDS tables. Other experimental values, such as the one of Zhang et al. (2003), are close to the value given by Wang et al. (1995). Taking the thermal expansion into account, one obtains the following values for ε, as $\varepsilon_{Wang} = 0.01938$ and $\varepsilon_{JCPDS} = 0.0105$.
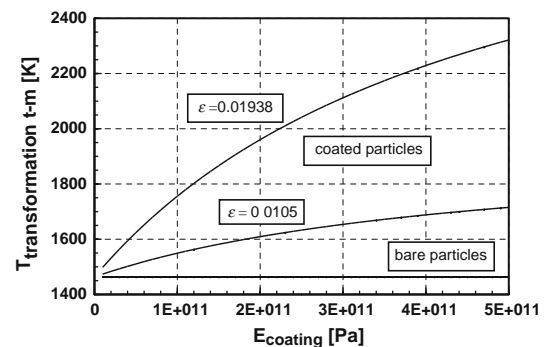
Figure 5. Temperature of the tetragonal $\to$ monoclinic transformation for bare and coated nanoparticles calculated on the basis of the thermodynamic data given by (Zhang et al., 2003) as a function of the Young's modulus of the coating. These results do obviously not describe the experimental results.

In the specimens used for PAC measurements, the particles had a radius of 2.5 nm and the coating a thickness of ca. 1 nm. Figure 5 gives the transformation temperature for bare and coated particles as a function of $E_{coating}$ and the different values of ε, calculated on the basis of equation (3). Figure 5 reveals a dramatic influence of the values selected for the volume change and transformation temperatures being far off the experimental values. This indicates that the values for the free enthalpy of transformation of coarse-grained materials are not applicable for nanoparticles.

Using $E_{coating}$ as a free parameter it is possible to evaluate equation (5) to estimate $\Delta H_{t \rightarrow m}$ and $\Delta S_{t \rightarrow m}$ as a function of $E_{coating}$. Additionally, as in the former case, two values were selected for ε. To analyse the sensitivity of the system with respect to the coating thickness, values of 0.75, 1.0, and 1.25 nm were selected. The results of these calculations are given in Figures 6 and 7. Again, the most striking result is the tremendous influence of the selection of ε, whereas the influence of the coating thickness is comparably marginal.

As a first approximation, for Young's modulus of amorphous alumina the one published by Zhang et al. (2003) for the crystalline material was selected. Using a value of 400 GPa (Wang et al., 1995; Asmani et al., 2001; Dorey et al., 2002) one obtains for $\Delta H_{t \rightarrow m}$ and $\Delta S_{t \rightarrow m}$ the values displayed in Table 5. Despite the uncertainty of $\Delta H_{t \rightarrow m}$ and $\Delta S_{t \rightarrow m}$, caused by the lack of sufficiently reliable data, the absolute values, derived from the comparison of the transformation temperature of bare and coated zirconia nanoparticles, are fundamentally different from the ones for coarse grained materials. Systematically, they show a change in the sign. Table 5 exhibits these values.

Even if it is only possible to show a trend, one difference is significant: The transition from coarse-grained to nanoparticulate material changes the sign of the thermodynamic functions $\Delta H_{t \rightarrow m}$ and $\Delta S_{t \rightarrow m}$. Indications into this direction were published earlier by Suresh et al. (2003) and Mayo et al. (2003). In the case of a particle size reduction from approximately 120 nm to 90 nm these authors found decreasing values of $\Delta H_{t \rightarrow m}$ by more than 15% for pure zirconia and of more than 20% for zirconia doped with Y. They estimate a critical diameter of 22.6 nm, where $\Delta G_{t \rightarrow m}$ is zero. Based on these results (Mayo et al., 2003) propose a grain size dependent phase diagram.

Besides the transformations, the structure of nanocrystalline cubic zirconia is the most interesting aspect. Even when X-ray and electron diffraction suggest a structure close to the cubic
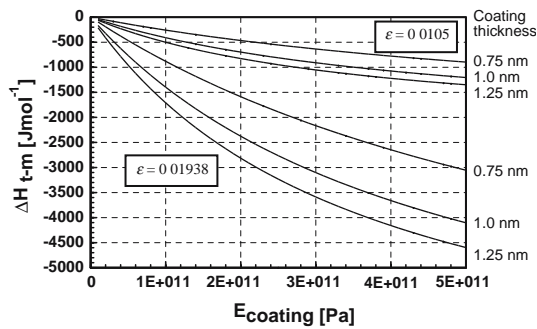

Figure 6. Enthalpy values for the tetragonal $\rightarrow$ monoclinic transformation of nanoparticulate zirconia estimated as a function of the Young's modulus of the coating for different assumptions of the volume change during trans formation.
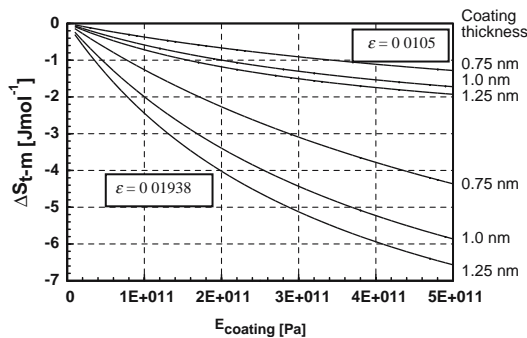

Figure 7. Entropy change for the tetragonal $\rightarrow$ monoclinic transformation of nanoparticulate zirconia estimated as a function of the Young's modulus of the coating for different assumptions of the volume change during trans formation.

Table 5. $\Delta H_{t \rightarrow m}$ and $\Delta S_{t \rightarrow m}$ values for coarse grained and nanoparticulate zirconia assuming a Young's modulus of 400 GPa for amorphous alumina

	$\Delta H_{t \rightarrow m}$ [Jmol^{-1}]	$\Delta S_{t \rightarrow m}$ [Jmol^{-1}K^{-1}]
Coarse grained material	6024	4.143
Nanoparticles, $\varepsilon_{JCPDS} = 0.0105$	-1000	-1.5
Nanoparticles, $\varepsilon_{Wang} = 0.01938$	-3500	-5.2

fluorite structure, PAC, EXAFS, and density measurements strongly indicate an unusual structure far away from the conventional one. PAC results give indications for a structure highly disordered with respect to the nearest neighbors. This finding is supported by the EXAFS results showing a structure with strong resemblance to the cubic fluorite structure and with drastically reduced coordination numbers for the Zr^{4+} ions with respect to the O and the next-nearest Zr shell. As a consequence of the reduced coordination numbers one expects a reduced density, which is confirmed by He-pycnometry.

These results together lead to the assumption that, taking an arbitrary Zr^{4+} ion, at least one or two out of eight neighbouring O^2 ions in the directly adjacent O shell and at least two out of twelve Zr^{4+} ions in the Zr shell are missing. The vacancies are not ordered; otherwise the PAC results should have shown a signal representing some symmetry. This is absolutely unusual. Normally, in coarse-grained materials, a structure with such a high content of vacancies would collapse as long as the vacancies were not forming a super-structure. This would be found easily in the X-ray or electron diffraction pattern. Additionally, PAC spectra reveal this symmetry, too. This defective cubic structure is not restricted to a material produced by the microwave plasma process; in fact, it was observed in a material produced by the gas condensation process (Forker et al., 1998), too. Earlier, Wang et al. (2004) found a cubic phase with distorted O-sublattice in thin films of zirconia with a thickness of less than 10 nm.

Nanocrystalline cubic zirconia is, at room temperature, not the only material showing this phenomenon. TiO_2 shows a disordered high temperature phase, too. Electron- and X-ray diffraction show that nanoparticulate TiO_2 with particle sizes around 3 nm crystallizes in the anatase structure (Schlabach et al., 2006). Similar as in the case of ZrO_2, the PAC spectra, however, indicate a disordered material. During grain growth, and before the transformation to the rutile phase, at a grain size of roughly 10 nm, the PAC spectra turn to the one of the crystallized phase. This gives an experimental size limit, for the existence of this disordered phase. Additionally, nanocrystalline Fe_2O_3 crystallizes in the cubic spinel structure, the γ-phase, exhibiting reduced density and coordination number, too. Similar to

Table 6. Density of nanocrystalline γ Fe_2O_3

	Nanoparticles (g cm^{-3})	X ray density (g cm^{-3})	Relative density of nanoparticles
γ Fe_2O_3	3.9	4.87	0.81

the cubic phase in zirconia, γ-Fe_2O_3 is the high temperature phase of Fe_2O_3. Table 6 displays density values determined by He-pycnometry.

The reduced density of nanocrystalline γ-Fe_2O_3 is caused by an increased number of vacancies leading to reduced coordination numbers. This was determined by EXAFS measurements, (Pellegrin et al., 1999). The results are shown in Table 7.

In this case, the reduced density and the reduced coordination numbers are not fitting, as in the case of cubic nano-zirconia. And there is a further similarity: In both cases, the radius of the O shell is reduced significantly, whereas the radii of the metal shells are nearly unchanged. Reduced density connected with high concentration of vacancies is not restricted to zirconia and iron oxide. This phenomenon was found in the cases of titania and hafnia, too. Table 8 shows a summary of these results.

A first explanation for this reduced density was presented by Ayyub et al. (1988) and they found an increase of the lattice parameter of γ-Fe_2O_3 when reducing the particle size from 18 to 8 nm, and for α-Fe_2O_3 by reduction the particle size from 50 to 30 nm. Additionally, the crystal field determined by Mößbauer spectroscopy was reduced in the case of the γ-phase from 53 to 45 T when reducing the particle size. In a later paper of this group, these authors report a similar tendency for γ-Al_2O_3 in the range from 10 to 20 nm, too (Ayyub et al., 1995). The authors (Ayyub et al., 1995) explain the lattice expansion by the termination of the particle surface by oxygen ions. As these ions have electric charge of equal sign, they repel each other. This leads to the lattice expansion. However, as the stoichiometry of the particles remains constant, an increased number of oxygen vacancies within the particle is necessary. Such a model leads eventually to particles of significantly reduced density. Based on a model first published by Sakai (1996) using Landau's ordering parameter, Chang and Johnson (2005) showed that for thermodynamic reasons tin nanoparticles with a particle size of ca. 4 nm have an ordering parameter of 0.6 in the center and 0.35 at the surface.

Table 7. Results of EXAFS measurements on nanocrystalline γ Fe_2O_3 with a particle size around 7 nm determined at room temperature (Pellegrin et al., 1999)

Shell	Experimental nano γ Fe_2O_3			Calculated γ Fe_2O_3 (Greaves, 1983)		
	Fe O	Fe Fe	Fe Fe	Fe O	Fe Fe	Fe Fe
Radial distance $\pm \sigma$ (nm)	0.193 ± 0.0011	0.30 ± 0.0011	0.344 ± 0.0011	0.198	0.296	0.347
Coordination number	4.7	3.1	3.3	5.25	6.0	7.1

Table 8. Density of nanocrystalline titania and hafnia in comparison to the X ray density

	Nanoparticles (g cm^{-3})	X ray density (g cm^{-3})	Relative density of nanoparticles	Particle size (nm)
TiO_2 rutile phase*	3.3	4.25	0.79	4
HfO_2 cubic phase	5.7	10.4	0.56	2 3

*Only a few of the specimens were pure rutile, the other ones contained anatas.

(This ordering parameter is defined as 1 for a crystallized system and 0 for a liquid.). As the theory of Chang and Johnson uses only surface and interface energies and the latent heat of fusion as input parameters, the results may be obtained for oxides, too.

Also the examples of TiO_2 and HfO_2 demonstrate a reduced density of the nanoparticulate material; even when the TiO_2 specimen contains anatas, the reduced density is striking. Crystallization in the phase of highest symmetry, which is, in general, the high temperature phase, was found by Ayyub et al. (1995) for Al_2O_3, Fe_2O_3, and for the more complex compounds $PbTiO_3$, $PbZrO_3$, $La_{1.85}Sr_{0.15}CuO_4$, $YBa_2Cu_3O_{7-\delta}$, and $Bi_2CaSr_2Cu_2O_8$ the same, too. Based on these results, for room temperature, these authors propose a new phase diagram, where the particle size is one of the main parameters. A similar variation of a generalized isothermal phase diagram was proposed by McHale et al. (1997). These authors plotted the enthalpy of formation vs. particle surface and found a stabilization of the γ-phase of Fe_2O_3 with increasing specific surface, that means with decreasing particle size. An extension of this work (Navrotsky, 2003) shows the same rules and modified phase diagrams governing Fe_2O_3 and ZrO_2, too. However, in case of zirconia, a direct transition from the tetragonal phase to an amorphous one was observed. Interestingly, Kao and Gorman (1990) found at room temperature up to 300°C an amorphous phase which transformed to the cubic phase. The cubic phase of zirconia was stable up to a temperature of 600°C. The appearance of the cubic phase with nanoparticulate zirconia was explained by the extreme small surface energy of the cubic phase.

In all the cases discussed above, a reduction of the particle size leads to a stabilization of the high temperature phase at room temperature. Obviously, in all of the discussed examples, nanoparticles – provided they are small enough – crystallize in the high temperature phase. This behavior reminds one of a generalized version of the p-T phase diagram proposed by Tammann (1903). This is sketched in a simplified version in Figure 8. The existence of this strange phase diagram was proven by findings of pressure-induced
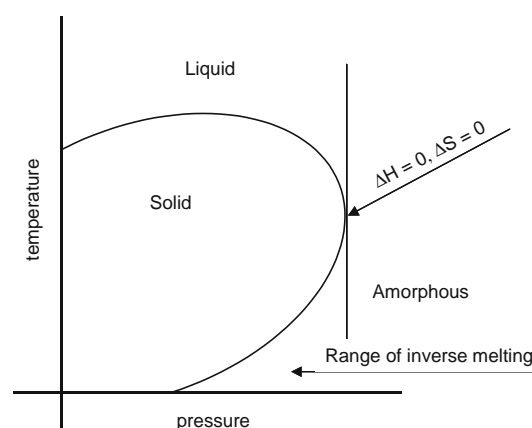

Figure 8. Simplified version of Tammann's pressure temperature phase diagram.

amorphization at constant temperature by Mishima et al. (1985) on ice and Hemley et al. (1988) on silica. The ultimate proof at constant pressure with increasing temperature was found by Rastogi et al. (1993, 1999) on organic compounds. A sound theoretical basis for Tammann's generalized phase diagram was given recently by Stillinger and Debenetti (2003) and Schupper and Shnerb (2005). Furthermore, (Ushakov et al., 2004) found for pure and La-doped zirconia and hafnia nanoparticles with a diameter of 5–6 nm that, at room temperature; the amorphous phase was more stable than the tetragonal one.

Based on the results demonstrated in this paper, in the case of zirconia one has to assume a generalization of Tammann's phase diagram (Tammann, 1903). A section of such a generalized phase diagram is shown in Figure 9. The part of the phase diagram that is realized experimentally is indicated in the graph. An important point in the phase diagram depicted in Figure 9 is the change of sign for $\Delta H_{t \to m}$ and $\Delta S_{t \to m}$. As shown in Table 5, this result is obtained by the comparison of the transformation temperatures of coarse-grained and nanoparticulate zirconia. This is in accordance with the predictions by (Tammann, 1903). Therefore, one may take the validity of a phase diagram similar to the one sketched in Figure 9 as granted. Except for the reversibility of the phase transformations, these results are identical with Ostwald's step rule (Ostwald, 1897) stating that a system will not reach the stable ground state directly, but will pass instead through
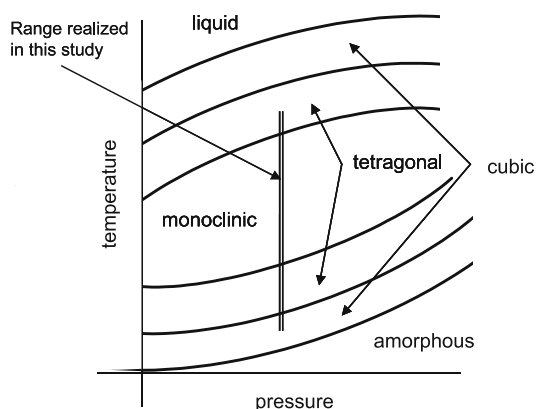
all less stable states, and with the Ostwald–Volmer rule (Volmer, 1983) stating that the high temperature phase is formed first.

Conclusions

The combination of PAC, electron diffraction, EXAFS, and He-pycnometry experimental techniques, providing information on local and global properties, has led to new insights into the structure and phase-relationship of zirconia nanoparticles. PAC has also been used to study the influence of the mechanical confinement of the particles by a coating with alumina on the phase transformations. The constraint exerted by the coating was found to provoke elastic strain energy due to a volume change during transformation and, therefore, leads to storage of this elastic strain energy that is "lost" for the phase transformation.

The main results are two new phenomena, not known for the coarse-grained compounds:

I. The as-produced zirconia, bare and coated, crystallizes in a structure close to the cubic fluorite structure, the high temperature phase of zirconia. However, this phase exhibits reduced density.

II. Heating cubic zirconia nanoparticles to temperatures above 500 K causes the transformation to the tetragonal and, at higher temperatures, to the monoclinic phase. The cubic to tetragonal transformation is partially reversible during cooling. Therefore, the cubic high temperature phase with high concentration of vacancies has to be considered as the equilibrium phase. The mechanical confinement of the zirconia particles by an alumina coating shifts the transformation temperature tetragonal – monoclinic from 700 K to 1300 K. The elastic strain energy, acting as transformation barrier, allows using these results to estimate the free enthalpy of this transformation. As the materials constants necessary for this evaluation are not known, it is only possible to give a rough estimate of $\Delta H_{t \to m}$, and $\Delta S_{t \to m}$.

In any case, these calculations show that both thermodynamic functions change sign when the particle size goes from coarse-grained material to a grain size around 5 nm.

Figure 9. Pressure temperature phase diagram for nanoparticulate zirconia with reference to Tammann's phase diagram as shown in Figure 8.

Comparable results were found for Fe_2O_3, TiO_2, HfO_2. In the open literature additional results on Al_2O_3, and a series of more complex oxides, showing the same behavior, are published. Additionally, a very detailed thermodynamical analysis of metallic nanoparticles teaches that small particles, may be with sizes below 10 nm are inherently disordered (Chang & Johnson, 2005). This size limit is in accordance with experimental results obtained on TiO_2. All results together support the assumption that nanoparticulate materials – provided the particles are sufficiently small – obey the following rules:

1. Compared to coarse-grained materials of the same structure, the density of nanoparticles is reduced.
2. Nanoparticles of materials showing phase transitions crystallize in the high temperature structure, but with reduced density.
3. Nanoparticles follow the generalized phase diagram postulated by Tammann.

Except for rule 1, these rules are compatible with Ostwald's step rule that a system will not reach the stable ground state directly, but – starting with the high temperature phase – passes through all less stable states instead. Until now, Tammann's p-T diagram has been confirmed only with organic materials. Probably, in this context, one also has to see the fact that some nanoparticles are – below a material dependent size – amorphous. Typical examples are Fe_2O_3 below 2 or 3 nm and Al_2O_3 below ca. 8 nm.

Acknowledgements

References

Antonioli G., P.P. Lottici, I. Manzini, G. Gnappi, A. Montenero, F. Paloschi & P. Parent, 1994. An EXAFS study of the local structure around Zr atoms in Y_2O_3 stabilized ZrO_2 by the sol gel method. J. Non Cryst. Solids 177, 179 186.

Asmani M., C. Kermel, A. Leriche & M. Ourak, 2001. Influence of porosity on Young's modulus and Poisson's ratio in alumina ceramics. J. Europ. Ceram. Soc. 21, 1081 1086.

Ayyub P., M. Multani, M. Barma, V.R. Palkar & R. Vijayaraghavan, 1988. Size induced structural phase transitions and hyperfine properties of microcrystalline Fe_2O_3. J. Phys. C, Solid State Phys. 21, 2229 2245.

Ayyub P., V.R. Palkar, S. Chattopadhay & M. Multani, 1995. Effect of crystal size reduction on lattice symmetry and cooperative properties. Phys. Rev. B 51, 6135 6138.

Bohm H.J., F.D. Fischer & G. Reisner, 1997. Evaluation of elastic strain energy of spheroidal inclusions with uniform volumetric and shear eigenstrains. Scripta Mater. 36, 1053 1059.

Catchen G.L., 1995. Perturbed angular correlation spectroscopy: renaissance of a nuclear technique. Mat. Res. Soc. Bull. 20, 37 46.

Chang J. & E. Johnson, 2005. Surface and bulk melting of small metal clusters. Phil. Mag. 85, 3617 3627.

Dorey R.A., J.A. Yeomans & P.A. Smith, 2002. Effect of pore clustering on the mechanical properties of ceramics. J. Europ. Ceram. Soc. 22, 403 409.

Fischer F.D. & E.R. Oberaigner, 2000. Deformation, stress state, and thermodynamic force for a transforming spherical inclusion in an elastic plastic material. ASME J. Appl. Mech. 67, 793 796.

Fischer F.D. & G. Reisner, 1998. A criterion for the martensitic transformation of a microregion in an elastic plastic material. Acta Mater. 46, 2095 2102.

Fischer F.D. & H.J. Bohm, 2005. On the role of the transformation eigenstrain in the growth or shrinkage of spheroidal isotropic precipitations. Acta Mater. 53, 367 374.

Forker M., J. Schmidberger, D.V. Szabó & D. Vollath, 2000. Perturbed angular correlation study of phase transformations in nanoscaled Al_2O_3 coated and noncoated ZrO_2 particles synthesized in a microwave plasma. Phys. Rev. B 61, 1014 1025.

Forker M., U. Brossmann & R. Wurschum, 1998. Perturbed angular correlation study of electric quadrupole interactions in nanocrystalline ZrO_2. Phys. Rev. B 57, 5177 5181.

Frauenfelder H., & R.M. Steffen, 1974. In: Siegbahn K. ed. Alpha, Beta, and Gamma Spectroscopy. North Holland, Amsterdam.

Garvie R.C., 1978. Stabilization of the tetragonal structure in zirconia microcrystals. J. Phys. Chem. 82, 218 224.

Greaves C., 1983. A powder neutron diffraction investigation of vacancy ordering and covalence in γ Fe_2O_3. J. Solid State Chem. 49, 325 333.

Hagelstein M., H.O. Moser, D. Vollath, C. Ferrero & M. Borowski, 2001. XAS investigation of Al_2O_3 coated nano composite ZrO_2. J. Synchrotron Radiation 8, 522 524.

Hemley R.J., A.P. Jephcoat, H.K. Mao, L.C. Ming & M.H. Manghnani, 1988. Pressure induced amorphization of crystalline silica. Nature 334, 52 54.

Inorganic Crystal Structure Database (ICSD) entry No. 4275.

Inorganic Crystal Structure Database (ICSD) entry No. 6814.

JCPDS #17 0923.

JCPDS #37 1484.

Kao A.S. & G.I. Gorman, 1990. Modification of zirconia film properties by low energy ion bombardment during reactive ion beam deposition. J. Appl. Phys. 67, 3826 3834.

Kingery W.D., H.K. Bowen & D.R. Uhlmann, 1976. Intro duction to Ceramics. John Wiley, Sons: New York.

Koningsberger D.C. & R. Prins eds., 1987. X Ray Absorption, Principles, Applications, Techniques of EXAFS, SEXAFS and XANES. John Wiley, Sons, New York, Vol. 92 in Chemical Analysis: A Series of Monographs on Analytical Chemistry and Its Applications.

Livey D. & P. Murray, 1956. Surface energies of solid oxides and carbides. J. Am. Ceram. Soc. 39, 363 372.

Massalski T.B., 1990. Binary Alloy Phase Diagrams, Vol. 3. ASM International, Metals Park Ohio.

Mayo M.J., A. Suresh & W.D. Porter, 2003. Thermodynamics for nanosystems: grain and particle size dependent phase diagrams. Rev. Adv. Mater. Sci. 5, 100 109.

McHale J.M., A. Auroux & A. Navrotsky, 1997. Surface energies and thermodynamic phase stability in nanocrystal line aluminas. Sci. Mag. 277, 788 791.

Mishima O., L.D. Calvert & E. Whally, 1985. An apparently first order transition between two amorphous phases of ice induced by pressure. Nature 314, 76 78.

Moulzolf S.C., Y. Yu, D.J. Frankel & R.J. Lad, 1997. Properties of ZrO_2 films on sapphire prepared by zyclotron resonance sputtering. J. Vac. Sci. Technol. A 15, 1211 1215.

Navrotsky A., 2003. Energetics of nanoparticle oxides: inter play between surface energy and polymorphism. Geochem. Trans. 4, 34 37.

Ondracek G., 1994. Werkstoffkunde: Leitfaden fur Studium und Praxis, Expert Verlag, Ehningen bei Boblingen.

Ostwald W. (1897). Studien uber die Bildung und Umwandlung fester Korper. Z. Phys. Chem. 22:289 302.

Pellegrin, Hagelstein E.M., Doyle S., Moser H.O., Fuchs J., Vollath D., Schuppler S., James M.A., Saxena S.S., Niesen L., Rogojanu O., Sawatzky G.A., Ferrero C., Borowski M., Tjernberg O., Brookes N.B. (1999). Characterization of nanocrystalline γ Fe2O3 with synchrotron radiation tech niques. Phys. Stat. Sol. B 215:797 801.

Rastogi S., Hohne G.W.H., Keller A. (1999). Unusual pressure induced phase behavior in crystalline poly(4 meth ylpentene 1); calorimetric and spectroscopic results and further implications. Macromolecules 32:8897 8909.

Rastogi S., Newman M., Keller A. (1993). Unusual pressure induced phase behavior in crystalline poly 4 methyl pentene 1. J. Polym. Sci. B 31:125 139.

Sakai H., 1996. Surface induced melting of small particles. Surf. Sci. 351, 285 291.

Schatz G. & A. Weidinger, 1996. Nuclear Condensed Matter Physics: Nuclear Methods and Applications. John Wiley & Sons, NewYorkJohn Wiley, Sons, New York .

Schlabach S., D. V. Szabó & D. Vollath, 2006. Structure and grain growth of TiO_2 nanoparticles investigated by electron and x ray diffraction and ^{181}Ta perturbed angular correla tions. J. Appl. Phys. (in the print).

Schupper N. & N. M. Shnerb, 2005. Condensed Matter. cond mat/0403674.

Srdic V.V., M. Winterer, G. Miehe & H. Hahn, 1999. Different zirconia alumina nanopowders by modifications of chemical vapor synthesis. NanoStruct. Mater. 12, 95 100.

Stillinger F.H. & G.P. Debenetti, 2003. Phase transitions, Kauzmann curves, and inverse melting. Biophys. Chem. 105, 211 220.

Suresh A., M.J. Mayo & W.D. Porter, 2003. Thermodynamics of the tetragonal to monoclinic phase transformation in fine and nanocrystalline yttria stabilized zirconia powders. J. Mater. Res. 18, 2912 2921.

Tammann G., 1903 Kristallisieren und Schmelzen. Ein Beitrag zur Lehre der Anderungen des Aggregatzustandes, Johann Ambrosius Barth, Leipzig.

Ushakov S.V., C.E. Brown & A. Navrotsky, 2004. Effect of La and Y on crystallization temperatures of hafnia and zirconia. J. Mater. Res. 19, 693 696.

Vollath D. & D.V. Szabó, 1994. Nanocoated particles: a special type of ceramic powder. NanoStruct. Mater. 4, 927 938.

Vollath D. & K.E. Sickafus, 1992. Synthesis of nanosized ceramic oxide powders by microwave plasma reactions. NanoStruct. Mater. 1, 427 437.

Vollath D., M. Forker, M. Hagelstein & D.V. Szabó, 2001. Structural disorder in the anion lattice of nanocrystalline zirconia and hafnia particles. Mat. Res. Soc. Symp. Proc. 634, B7.7.1 B8.2.

Volmer M., 1983. Zur Kinetik der Phasenbildung und Elek trodenreaktion. Harri Deutsch, Frankfurt/M.

Wang C.M., S. Azad, S. Thevuthasan, V. Shuttanandan, D.E. McCready & C.H.F. Peden, 2004. Distortion of the oxygen sublattice in pure cubic ZrO2. J. Mater Res. 19, 1315 1319.

Wang Y.S., C. He, B.J. Hockey, P.I. Lacey & S.M. Hsu, 1995. Wear transitions in monolithic alumina and zirconia alumina composites. Wear 181 183, 156 164.

Zhang Y.L., X.J. Jin & T.Y. Hsu, 2003. Thermodynamic calculation of M_s in ZrO_2 CeO_2 Y_2O_3 system. J. Europ. Ceram. Soc. 23, 685 690.